construction materials

MDPI

Article

Characterization of Carbonated and Raw Ferronickel Slags as Cementing Materials

Priscillia Laniesse [1], Adrien Dufourny [2], Florent Bourgeois [2], Carine Julcour [2] and Martin Cyr [1,*]

[1] LMDC, Université Paul Sabatier, 31400 Toulouse, France
[2] Laboratoire de Génie Chimique, Université de Toulouse, CNRS, INPT, UPS, 31400 Toulouse, France; florent.bourgeois@toulouse-inp.fr (F.B.); carine.julcour@toulouse-inp.fr (C.J.)
* Correspondence: cyr@insa-toulouse.fr

Abstract: This study's aim is to fully characterize ferronickel slag from New Caledonia, considered a multiphase mineral containing amorphous material. The methodology consisted of combining chemical, mineral, and morphological characterization techniques, such as ICP-AES, TGA, Q-XRD, microscopy, spectroscopy, etc. The ferronickel slag consisted of 44 wt. % forsterite, with the inclusion of iron as a substitution for magnesium ($Mg_{1.8}Fe_{0.2}SiO_4$), 1.7 wt. % chromite and 54 wt. % amorphous phase containing iron, magnesium, aluminum, and silica (Mg/Si = 0.4; Fe/Si = 0.2; Al/Si = 0.1). This material was slightly reactive in a cementitious medium, thus limiting its use as an SCM in the construction sector. The ferronickel slag was then subjected to an attrition-leaching carbonation process at 180 °C and a partial pressure of CO_2 of 20 bar. The obtained product, carbonated at 80% of its capacity, was also characterized. It was composed of carbonates (37% of magnesite and 4% of siderite), remaining forsterite (7 wt. %), chromite (1 wt. %), and 50% of an amorphous phase, mainly composed of silica and aluminum. The complete characterization of those products helped in understanding the chemistry of the carbonation process and finding valorization paths for the carbonated products in the construction sector. The carbonated product may be used either as an SCM in blended cement or as a precursor of magnesium–silicate binders.

Keywords: characterization; ferronickel slag; magnesium silicates; amorphous phase; carbonated products; waste valorization

Citation: Laniesse, P.; Dufourny, A.; Bourgeois, F.; Julcour, C.; Cyr, M. Characterization of Carbonated and Raw Ferronickel Slags as Cementing Materials. *Constr. Mater.* **2024**, *4*, 524–542. https://doi.org/10.3390/constrmater4030028

Received: 21 April 2024
Revised: 30 June 2024
Accepted: 19 July 2024
Published: 1 August 2024

1. Introduction

Globally, carbon dioxide emissions have now reached 43 GT/year [1], and it is becoming urgent to reduce CO_2 emissions, especially in the construction sector, which is the world's second-largest industrial CO_2 emitter [1]. One of the most efficient strategies proposed to reduce the environmental impact of the cement industry is to reuse waste materials as supplementary cementing materials (SCMs). The best-known and most widely used SCMs are fly ash, ground granulated blast furnace slag (GGBS), and silica fumes [2,3]. However, these traditional SCMs are not available everywhere, and for most of them, their amount is significantly lower than the amount of cement required in the construction sector. Therefore, it is highly necessary to study and develop new SCMs.

Ferronickel slag is a by-product of ferronickel production with the pyrometallurgical process, either in a blast furnace or an electric arc furnace [4]. In New Caledonia, around 2 million tons of ferronickel slags is discharged annually, but only 8% is reused [5]. The chemical composition of the ferronickel slag depends on the process and temperatures; however, it mainly includes SiO_2, MgO, CaO, Al_2O_3, and Fe_2O_3 [6,7], while the mineralogical composition primarily includes olivine and serpentine. When the ferronickel slags are quenched with water, the content of the amorphous phases is usually greater than 50% [8].

As it occupies a large area of the land and might be harmful to the environment, ferronickel slag should be valorized and reused. Several industrial applications of these

ferronickel slags have been suggested [9]. For instance, they can be used as mineral admixtures for several types of binders such as phospho-magnesian cements (MKP), geopolymers, or calcium-silicate cements [6,10–12]. However, the use of these slags as SCMs is of little interest, as MKP cements and geopolymers are not widely used, and their production is expensive; therefore, these two binders would not permit a sufficient re-utilization of ferronickel slag. Furthermore, their use as an SCM as a replacement for Portland cement could be relatively poor, due to the low reactivity of the product. Ferronickel slag could also be used as raw material to synthetize calcium silicate cements [13], but, here again, the utility is limited due to the need for other natural minerals or industrial by-products, such as fly ash or blast furnace slag, to increase the amount of calcium, which are not available in New Caledonia. The use of ferronickel slags as molding sand or aggregates for concrete is, for now, the most promising application [14,15], because they have proven their reliability for the utilization without apparent deleterious ASR expansion risk, although the fraction of glassy phase is high [16].

Another solution to reuse ferronickel slag might be through its carbonation. In fact, the presence of magnesium silicate makes the mineral very inert, impacting the bearing capacity development for structures. The carbonation of such materials has several advantages [17]:

1. Capture and stable storage of carbon dioxide inside a material.
2. Separation of magnesium from silica in two distinct minerals: magnesite ($MgCO_3$) and silica (SiO_2). This might lead to a higher reactivity of the silica fraction with calcium in cementitious materials.

However, to optimize the carbonation process and the valorization path of the final product, it is important to know both the initial and final product properties. The objective of this study is to describe a full characterization path for a specific ferronickel slag from New Caledonia and one carbonation product, obtained using an attrition-leaching aqueous process [18].

The full characterization of multiphase minerals requires the use of a panel of analytical techniques, for instance, spectroscopy, elemental composition, XRD, or TGA. Each technique characterizes one part of the sample. However, in the literature, authors often characterize the chemical composition and mineralogy of crystalline phases, leaving the characterization of amorphous materials behind. The characterization of amorphous phases is usually more complex than that of crystalline materials, especially in complex multiphasic minerals. In addition, this characterization often uses specific unusual techniques that are scarce, expensive, or require qualified experimentalists. The objective of this study is to propose a characterization path for multiphase minerals, including crystalline and amorphous phases, using usual laboratory techniques as much as possible. As the amorphous phase is responsible for the pozzolanic reactivity of SCMs, its characterization could help better explain the value of the carbonation process of such materials.

In this study, the authors propose a full characterization path of both native ferronickel slag from New Caledonia and carbonated products to evaluate their use as SCMs in cement-based materials.

2. Materials and Methods

2.1. Feedstock and Carbonation Process

2.1.1. Feedstock Origins

In this study, the feedstock was ferronickel slag from "Le Nickel" company in New Caledonia. This French overseas territory in the Pacific is the world's first ferronickel manufacturer, one of two pyrometallurgic factories that produce ferronickel from garnierite ($3NiO{\cdot}3MgO{\cdot}2SiO_2{\cdot}2H_2O$) in electric arc furnaces [19]. Ferronickel slag is a by-product resulting from the manufacturing process of ferronickel. According to Huang et al. [20], this type of slag contains three main oxides: MgO, Fe_2O_3 and SiO_2. The blast furnace slag can be either quenched by sea water (fast cooling) or cooled at ambient air temperature (slow cooling). The cooling method will mainly affect the crystallinity of the slag. This work focuses on water-quenched ferronickel slag from New Caledonia.

This type of material mostly includes magnesium silicates, either crystalline or amorphous. Therefore, its carbonation will likely result in the formation of magnesium carbonate and amorphous silica [17].

2.1.2. Direct Aqueous Carbonation of the Ferronickel Slag Using an Attrition-Leaching Process

The attrition-leaching process used in this study is detailed in the following papers, so only the main steps are outlined in [17,21]. The carbonation reaction here takes place in aqueous phase using a laboratory 300 mL autoclave operated as an attrition-leaching reactor; it contains a bed of millimeter-sized grinding beads stirred by a pin-drive impeller. This device enables one to control both pressure and temperature, with a continuous attrition of the slag particles to remove leached layers. The reactor has a diameter of 60 mm and a height of 100 mm and is heated by an annular furnace. The slurry temperature is measured with a Pt100 probe inserted in an immersion sleeve. The pressure is measured by a piezoresistive transmitter (Keller PA-23SY) and is set by a membrane pressure regulator connected to a pressurized CO_2 gas bottle. A more detailed description of the reactor is provided by Dufourny et al. [22]. The temperature and pressure are kept constant during the whole reaction. In the investigated conditions, the temperature is maintained at 180 °C and CO_2 partial pressure at 20 bar. Pure CO_2 is used in all experiments reported in this study. The attrition is performed with 1 mm yttrium-stabilized zirconia beads (Netsch Zetabeads Plus) agitated at 500 rpm, which corresponds to an impeller tip speed of 1.38 $m \cdot s^{-1}$. In the reactor, 540 g of zirconium balls is mixed with 8 g of native slag (grounded at a particle size lower than 100 µm) and 80 g of distilled water. The filling rate of the reactor is then around 70%. The reaction lasts 24 h. Then, the whole reactor content is sieved on a 0.8 mm mesh screen and rinsed with distilled water to separate the grinding beads from the slurry. The collected suspension is centrifuged, and the solid residue is finally dried at 105 °C for 24 h. It is manually ground in an agate mortar and dry-sieved below 80 µm before further characterization.

2.2. Analytical Techniques

The full characterization of minerals requires the use of a panel of analytical techniques to determine their chemical composition, as well as mineralogy and physical properties.

2.2.1. Determination of the Elemental Composition

The elementary composition of the ferronickel slag was characterized by ICP-AES after total alkaline digestion of the materials. The digestion method made use of a melting agent composed of 35% of lithium tetraborate (LiB_4O_7) and 65% of lithium metaborate ($LiBO_2$). The ratio of the components in the melting agent is different than the 50:50 classical ratio, because it makes the digestion of silicates easier. Next, 200 mg of the sample was mixed with 1.2 g of melting agent in a graphite crucible. Then, the crucible was placed in an oven at 1100 °C for one hour. HNO_3 solution (5%) was added to the molten mixture in a beaker and agitated overnight until complete dissolution of the fusion bead. Finally, the solution was filtrated on a slow quantitative filter and rinsed 7 times with ultra-pure water. ICP-AES was performed on a Perkin Element Optima 7000 DV apparatus.

The loss of ignition was measured after heating the samples at 1100 °C for one hour in a laboratory muffle furnace.

The measurement of carbon and water content was carried out using thermogravimetric analysis coupled with mass spectroscopy (TGA-MS). Experiments were performed on samples heated up to 1000 °C at a constant rate of 10 °C/min, under air atmosphere (gas flow set at 50 mL/min), with a Netzsch STA 449 F3/F1 Jupiter instrument. For this experiment, 5 mL aluminum oxide crucibles were used. All curves were corrected for buoyancy effects (caused by the density of the surrounding gas decreasing on heating) by performing a blank subtraction.

2.2.2. Characterization of the Mineralogy

Crystalline phases were characterized using X-ray diffraction (XRD) technique. Experiments were carried out on a Bruker D8 Advance machine, using a copper X-ray anode ($\lambda_{K\alpha 1}$ = 1.5418 Å) as X-ray source and equipped with a vertical theta/theta goniometer and a LynxEye XE-TTM high-speed linear detector. A motorized anti-scattering knife was used to attenuate direct radiation. Diagrams were acquired at 40 kV and 40 mA, from 7° to 70°, with a step of 0.02° and a total acquisition time of 2 h 30 min. For this analysis, the samples were further ground in an agate mortar and sieved below 40 µm. Mineral identification was performed using the Bruker-AXS DIFFRACplus Eva v4 software and the 2015 ICDD PDF database.

To obtain the quantitative evolution of the phases during the hydration process, Rietveld mineralogical modelling calculations were performed using the DIFFRACplus Topas v5 software (Bruker-AXS, Karlsruhe, Germany). To quantify the amorphous fraction in samples, the external standard method was used. The choice of the standard requires one to know the chemical composition of the samples to calculate their Mass Attenuation Coefficient (MAC); the standard's MAC should be close to the one of the samples.

The MAC of both samples was calculated by summing the MAC of their element oxides (Equation (1)) at the energy of the X-ray tube (here, 8.04 keV (copper)). The MACs of these oxides are given in Table 1 [23].

$$\mu_{samp} = \sum_i w_i \cdot \mu_i \quad (1)$$

Table 1. Mass Attenuation Coefficient (MAC) of oxides entering slag elemental composition.

	MgO	**SiO_2**	**Al_2O_3**	**CaO**	**Fe_2O_3**	**Cr_2O_3**	**MnO**	**ZrO_2**	**H_2O**	**CO_2**
MAC (m^2/kg)	29.0	36.4	32.1	125.9	217.4	175.6	214.4	103.3	10.3	9.6

The MACs of standards that are classically used in XRD are given in Table 2 for a comparison to the ones of the samples.

Table 2. MAC of external standards classically used for Rietveld refinement.

	Quartz (SiO_2)	**Corundum (Al_2O_3)**	**Rutile/Anatase (TiO_2)**	**Zincite (ZnO)**	**Fluorite (CaF_2)**
MAC	36.0	30.9	124.2	49.3	89.8

The evaluation of the "normalization constant" of the external standard (the so-called K-factor) required, in the first place, to acquire the X-ray diagram of the standard alone. The K-factor was then deduced from the measured scale factor (S_{std}) according to Equation (2).

$$K = \frac{S_{std} \times \rho_{std} \times V_{std}^2 \times \mu_{std}}{W_{std}} \quad (2)$$

where ρ_{std} is the standard density, V_{std} is the standard's unit cell volume, μ_{std} is the standard MAC, and W_{std} is the weight ratio of the standard, here equal to 1.

The K-factor was entered into Topas software when the Rietveld refinement was carried out on the sample diffractogram, and the absolute weight fraction of each known phase was then calculated using Equation (3).

$$W_{\alpha(abs)} = \frac{S_\alpha \times \rho_\alpha \times V_\alpha^2 \times \mu_{sample}}{K} \quad (3)$$

where S_α is the scale factor of phase α and μ_{sample} is the MAC of the entire sample.

Two parameters were analyzed as fitting criteria: the Goodness of Fit (GOF) and the weight residuals of pattern (Rwp) [24]. For a good fit, the GOF should be less than 10 and the Rwp inferior to 15.

XRD gave information on the composition of the crystalline phases and on the total amount of amorphous phases but not on the variability and composition of the amorphous phases. Therefore, a spectroscopic method was needed to complete the mineralogical characterization. Here, Fourier-transform infrared (FT-IR) analysis was used as a complementary tool to characterize both crystalline and amorphous phases. Spectra were acquired on a Perkin Elmer instrument. The analysis was performed in reflexion mode on a diamond crystal over a wavelength range from 500 to 4000 cm^{-1}. Spectra were then compared to those of pure compounds reported in the literature.

2.2.3. Microstructure

The specific surface area of the (carbonated) slag was measured by the Brunauer–Emmett–Teller (BET) method on a Belsorp-Max device, using nitrogen absorption at 77.4 K on about 1.5 g of sample. Before the measurement, the solid samples were pre-treated under vacuum at 120 °C for 10 h in a Belprep-Vac II apparatus. Their density was determined with a helium pycnometer (Micrometrics AccuPyc 1330) of 1 cm^3 capacity.

The microstructure of the native slag was observed using a MEB/FIB FEI HELIOS 600i Scanning Electronic Microscope (SEM). The device was equipped with a Field-Emission Gun (FEG), a gallium ion column, and an Energy-Dispersive X-ray Spectroscopy (EDS) detector. The images were acquired at an acceleration voltage of 15 kV with the Back-Scattered Electron (BSE) detector in order to differentiate the phases by their elemental composition (the lighter the image, the heavier the atoms). A current of 1.4 nA and at a working distance of 4 mm were applied. Then, a slice of the sample was cut using the Focused Ion Beam (FIB) containing gallium ions (Figure 1) and was thinned to become transparent to electrons.

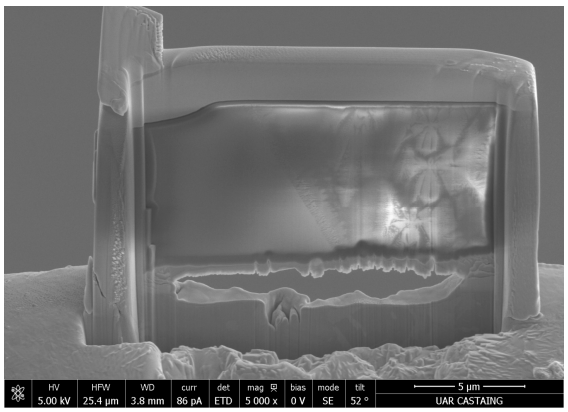

Figure 1. Cutting of a thin slice of the native slag by FIB.

The FIB lamella was observed with a TEM JEOL JEM 2100F Transmission Electron Microscope (TEM) equipped with an EDS detector. TEM images were acquired at 200 kV. The microscope resolution was 2.3 Å. Different interesting areas were selected to perform X-ray diffraction and EDS analyses. Scanning mode (STEM) was also applied for elemental mapping. Note that the native slag was not affected by the electrons.

As for the carbonated slag, only TEM analysis was performed, as its particles were too small to be properly investigated by SEM. The powder was dispersed in ethanol under ultrasound for several minutes; then, a drop was placed on a TEM copper grid covered with a carbon film. The sample was analyzed after the evaporation of the solvent.

3. Results

3.1. Chemical Analysis

The chemical composition of the feedstock was determined as a first step to improve the accuracy of the mineralogical characterization by XRD. In addition, having quantitative information on the sample chemistry allows for verification of the Rietveld refinement results and enables a mass balance to determine the composition of the amorphous phase. The results of ICP-AES and loss-of-ignition analysis are given in Table 3.

Table 3. Oxide composition of native and carbonated slags obtained from ICP-AES analysis (absolute measurement error in brackets).

	MgO	SiO_2	Al_2O_3	CaO	Fe_2O_3	Cr_2O_3	MnO	ZrO_2	L.O.I	Total
Ferronickel slag	31.2 (1.6)	52.6 (2.6)	2.7 (0.1)	0.70 (0.03)	12.4 (0.6)	1.10 (0.05)	0.20 (0.02)	<D.L.	<D.L.	101.2 (5.0)
Carbonated slag	20.3 (1.0)	35.6 (1.8)	2.8 (0.1)	1.21 (0.06)	10.4 (0.5)	0.86 (0.04)	0.35 (0.02)	1.24 (0.06)	30.3 (1.5)	103.5 (5.1)

As some elements could not be analyzed by ICP-AES (such as hydrogen, carbon, nitrogen, etc.), thermogravimetric analysis coupled with mass spectroscopy (TGA-MS) was used to quantify the amounts of CO_2, H_2O, and SO_2. It should be first noticed that the native slag did not exhibit any significant mass loss up to 1000 °C (<0.5%). Only two compounds were responsible for the mass loss on the carbonated samples: water and carbon dioxide. The loss of water occurred mainly between 30 and 300 °C, whereas decarbonation occurred from around 300 °C to 700 °C, as shown in Figure 2. Table 4 summarizes the corresponding results. The L.O.I (30.3%) and the total TGA mass loss (27.4%) were slightly different; this small discrepancy could be ascribed to the difference in the final temperature (1000 °C for TGA and 1100 °C for L.O.I) and the fact that with L.O.I, there is a 1 h plateau at 1100 °C, whereas the TGA experiment ends when the sample reaches 1000 °C. The loss of water is likely related to hydrated amorphous silica, an expected product of the carbonation process of magnesium silicate minerals. A small loss of carbon dioxide was detected around 200 °C, which was probably due to the presence of organic residue from the carbonation process (the reactor including a PEEK liner).

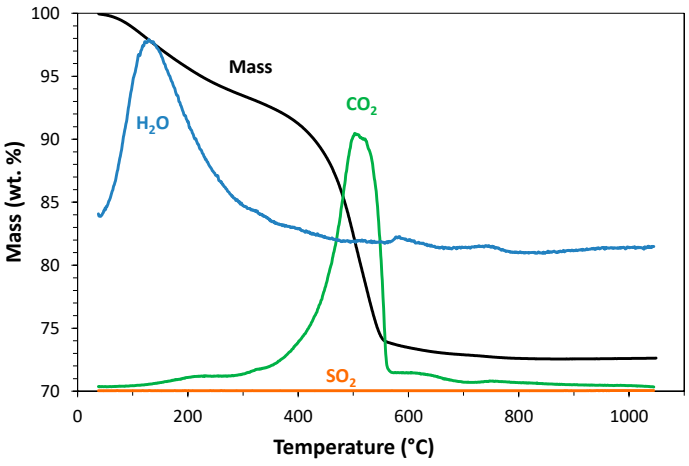

Figure 2. TGA-MS curves of a carbonated slag.

Table 4. Mass loss from TGA of the carbonated slag (and detected gas).

Temperature Range (°C)	Mass Loss (wt. %)	Detected Gas
30–1100 °C	27.4%	$H_2O + CO_2$
30–300 °C	6.7%	H_2O (CO_2)
300–600 °C	20.7%	CO_2

3.2. Mineralogy

3.2.1. XRD and Rietveld Analysis

First, the X-ray diagrams of the native and carbonated ferronickel slag samples were acquired (results in Figure 3), and the phases were determined according to their elemental composition. The native slag contains one major crystalline phase: forsterite ferroan ($(Mg,Fe)_2SiO_4$). This is a naturally occurring magnesium silicate, from the olivine family, in which some of the magnesium cations are substituted by iron (II). Also, clinoenstatite ($MgSiO_3$) was observed, a magnesium silicate from the pyroxene family. In the carbonated slag, three crystalline phases were characterized, unreacted forsterite iron from the native slag, magnesite ($MgCO_3$), and siderite ($FeCO_3$), which are the carbonated products. Nonetheless, the crystalline peaks of magnesite and siderite being very close, it is difficult to distinguish whether the sample is composed of the separate carbonates and/or a mixed $(Mg,Fe)CO_3$ phase.

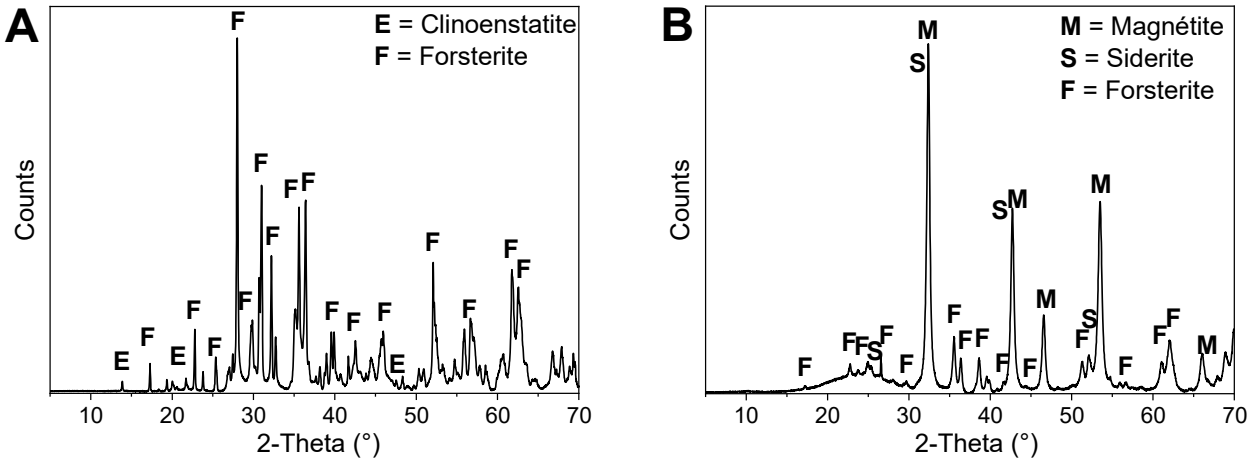

Figure 3. X-ray diffractograms of (**A**) native slag and (**B**) carbonated slag.

Then, Rietveld refinement was performed to calculate the amount of each crystalline phase and the total amount of the glassy phase (the fits are given in Figure 4). Based on their oxide composition, the calculated MACs of ferronickel slag and carbonated product are 59.2 and 44.5 $m^2 \cdot kg^{-1}$, respectively. Thus, zincite was chosen as the external standard for both samples to perform Rietveld refinement.

According to these results, the native slag contains around 45% of forsterite, a small amount of enstatite, and 55% of amorphous materials. As for the carbonated slag, it contains about 7% of residual forsterite, 37% of magnesite, 4% of siderite, and around 50% of amorphous materials (see Table 5). For both samples, Rietveld refinements were accurate since the GOF was lower than 3.5 and the RWP lower than 5.

Table 5. Rietveld refinement results for the native and carbonated slags.

	Native Slag	**Carbonated Slag**
% Forsterite iron	44.1 ± 0.6	7.0 ± 0.6
% Clinoenstatite	0.4 ± 0.3	-
% Magnesite	-	37.3 ± 0.7
% Siderite	-	3.6 ± 0.3
% Residual: amorphous and undetected crystalline phases	55.4 ± 0.6	52.1 ± 1.0

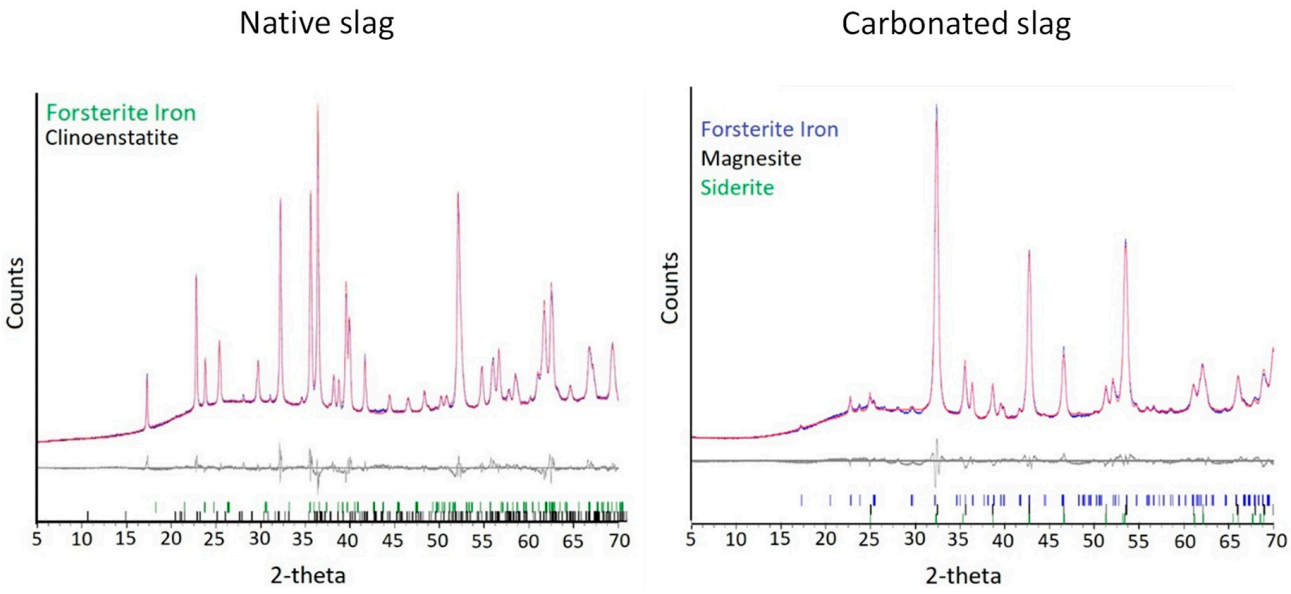

Figure 4. Results of Rietveld refinement for the native slag (**left**) and carbonated slag (**right**) (blue = measured diagram; red = diagram calculated with Rietveld refinement and grey = residual pattern).

The absolute errors given in Table 5 are those obtained from the calculation. However, the usual uncertainty of a Rietveld refinement is generally around 2–5%, so higher than the ones given by the software. The accuracy of results obtained by Rietveld refinement was evaluated by the comparison between the number of carbonates and carbon dioxide content measured by TGA (see Section 3.1).

Finally, the Rietveld refinement also enabled us to calculate the ratio of magnesium to iron in the forsterite iron phase. The forsterite formula is then $Mg_{1.8}Fe_{0.2}SiO_4$.

3.2.2. Mass Balances

The XRD analysis of the native and carbonated slags revealed an important amount of amorphous phase in both samples. Elemental balances and FT-IR were then used as complementary tools to evaluate their stoichiometric composition.

The elemental composition of the glassy phases could be deduced by combining the results from ICP-AES, TGA, and the Rietveld refinement of the diffraction patterns. In addition, chromium, whose bearing phase could not be detected by XRD, was ascribed to chromite ($FeCr_2O_4$) only, following the conclusions of an internal analysis report. The amount of this mineral was then calculated using the total amount of chromium determined by ICP-AES and subtracted to the residual phase content after Rietveld refinement. The results are given in Tables 6 and 7 for the native and carbonated slag, respectively.

The calculations showed that the amorphous phase in the native slag contained primarily SiO_2 and (MgO + FeO), with a molar ratio around 2. It also included a small fraction of aluminum. The calculated atomic ratios in the amorphous phase were Mg/Si = 0.42; Fe/Si = 0.07; Al/Si = 0.04.

As for the carbonated slag, the amorphous phase contained a significant amount of silica and water, with small amounts of iron and aluminum. As mentioned above, the reaction of magnesium silicates with dissolved CO_2 resulted in magnesium and iron carbonates, as well as partially hydrated amorphous silica.

Mass balances made it possible to calculate the composition of the amorphous part of the sample, but it did not yield its chemical nature and variability.

Table 6. Mass balance results for the native slag.

Mineral	Chemical Formula	Proportion	Oxide Formula	Oxide (wt. %)	Oxide (mol. %)
Forsterite	$Mg_{1.8}Fe_{0.2}SiO_4$	44.1	MgO	21.4	44.2
			Fe_2O_3	5.2	2.7
			SiO_2	18.0	24.8
Clinoenstatite	$MgSiO_3$	0.4	MgO	0.2	0.3
			SiO_2	0.2	0.3
Chromite	$FeCr_2O_4$	1.7	Fe_2O_3	0.6	0.3
			Cr_2O_3	1.1	0.7
Amorphous	Unknown	53.8	MgO	9.6	20.0
			Fe_2O_3	6.5	3.4
			SiO_2	34.3	47.3
			Al_2O_3	2.7	2.1
			MnO	0.2	0.2
			CaO	0.7	1.0

Table 7. Mass balance results for the carbonated slag.

Mineral	Chemical Formula	Proportion	Oxide Formula	Oxide (wt. %)	Oxide (mol. %)
Forsterite	$Mg_{1.8}Fe_{0.2}SiO_4$	7.0	MgO	3.6	5.6
			Fe_2O_3	0.5	0.2
			SiO_2	2.9	2.9
Chromite	$FeCr_2O_4$	1.1	Fe_2O_3	0.4	0.2
			Cr_2O_3	0.9	0.3
Magnesite	$MgCO_3$	37.3	MgO	17.8	27.3
			CO_2	19.5	27.3
Siderite	$FeCO_3$	3.6	Fe_2O_3	2.5	1.0
			CO_2	1.4	1.9
Amorphous	?	51.0	SiO_2	32.7	33.5
			Fe_2O_3	7.0	2.7
			Al_2O_3	2.8	1.7
			MnO	0.2	0.1
			CaO	1.2	1.3
			H_2O	6.7	29.4

3.2.3. FT-IR

In order to identify other materials in addition to crystalline phases, FT-IR was used. By using this technique, the minerals can be differentiated via the characteristic vibrational properties of their atomic bonds. Although this provides the opportunity to identify amorphous silica or saponite-like phases, it is sometimes limited when the minerals hold the same chemical bonds and, thus, the same characteristic vibrations, such as enstatite or forsterite, which are both magnesium silicates. The sample spectra were compared to those of pure phases from the literature in order to help their identification.

Figure 5A shows the FT-IR spectrum of the native slag, typical of a forsterite (Mg_2SiO_4) phase [25,26]. Peaks around 500 cm^{-1} and 620 cm^{-1} correspond to the bending vibrations of the Si-O groups, while peaks in the range 830–1000 cm^{-1} are associated with stretching

vibrations of the Si-O groups. It should be noted that FT-IR did not help differentiate the amorphous phase and forsterite, since they are both magnesium silicate phases displaying the same bounding vibrations.

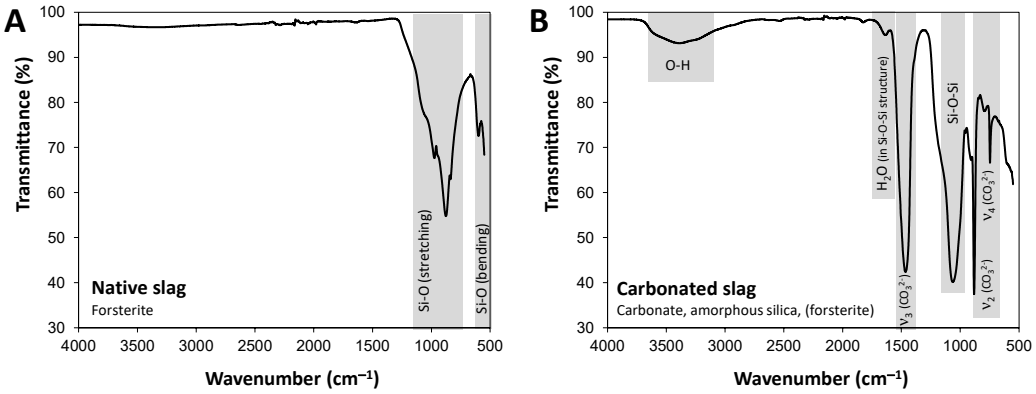

Figure 5. FT-IR spectra of (**A**) native slag and (**B**) carbonated slag.

Figure 5B shows the FT-IR spectrum of the carbonated slag, with magnesite ($MgCO_3$) having strong carbonate absorption bands around 880–885, 1450–1470, and 745–750 cm^{-1} for ν_2, ν_3, and ν_4 modes, respectively [27–29]. The presence of amorphous hydrated silica was evidence, via absorption bands characteristic of the Si-O-Si groups (1000–1100 cm^{-1}), the stretching vibrations of O-H groups (3300–3500 cm^{-1}), and molecular coordinated water within the SiO_2 structure (1600–1650 cm^{-1}) [30].

3.2.4. Electron Microscopy Coupled to Elemental Analysis (SEM- and TEM-EDS)

The native and carbonated slags were analyzed using electron microscopy (SEM and TEM) coupled to EDS. The objectives of these analyses were as follows:

1. To confirm the composition of the forsterite (1.8 MgO/0.2 FeO);
2. To analyze the amorphous material in terms of elemental composition and variability;
3. To observe the carbonates in the carbonated slag, either as separate magnesite and siderite or as a $(Mg,Fe)CO_3$ solid solution.

SEM observations were carried out on both the native and carbonated samples (Figure 6). The BSE of a polished section of resin-coated native slag (Figure 6A) made it possible to observe different morphologies: large particles which appear in the dark (therefore, made of light elements) and seem to be porous, needle-like particles containing crystallites, and a third phase, including the other two phases, which is lighter. In terms of composition, the results of EDS were inconclusive due to the intimate imbrication of the mineral phases. For the carbonated slag (Figure 6B), the SEM image made on a powdered sample showed that each grain was composed of an agglomeration of submicronic particles. Therefore, TEM observations were carried out to analyze both materials in greater detail.

Native Slag

The electron diffraction mode in TEM was used to discriminate crystalline and amorphous phases (on the diffraction pattern, dots count for crystalline phases and halo ring for the amorphous phase) and the scanning mode (STEM) was used to determine the elemental composition of the three different highlighted zones, labelled A to C in Figure 7. As seen from the corresponding diffraction pattern, A is 100% amorphous and contains mostly silica (see elemental mapping at the bottom of Figure 7), while B and C are 100% crystalline but show different chemical compositions: B is mostly composed of magnesium, while C also contains a significant amount of silica. In addition to elemental mapping using STEM-EDS, quantitative EDS analysis was also performed pointwise on several areas for each sample.

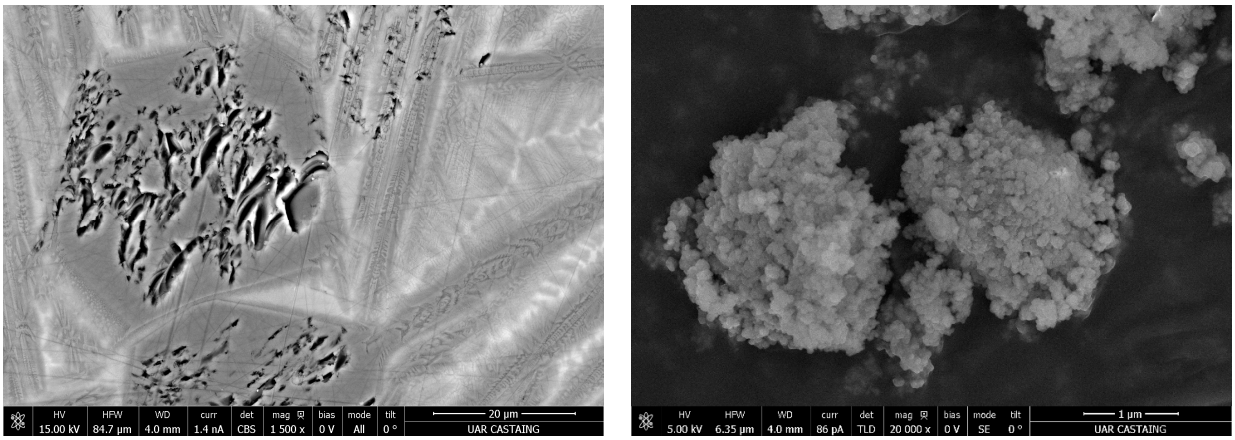

(**A**) (**B**)

Figure 6. SEM images (BSE, 15kV) of (**A**) a polished section of the native slag and (**B**) the carbonated slag powder.

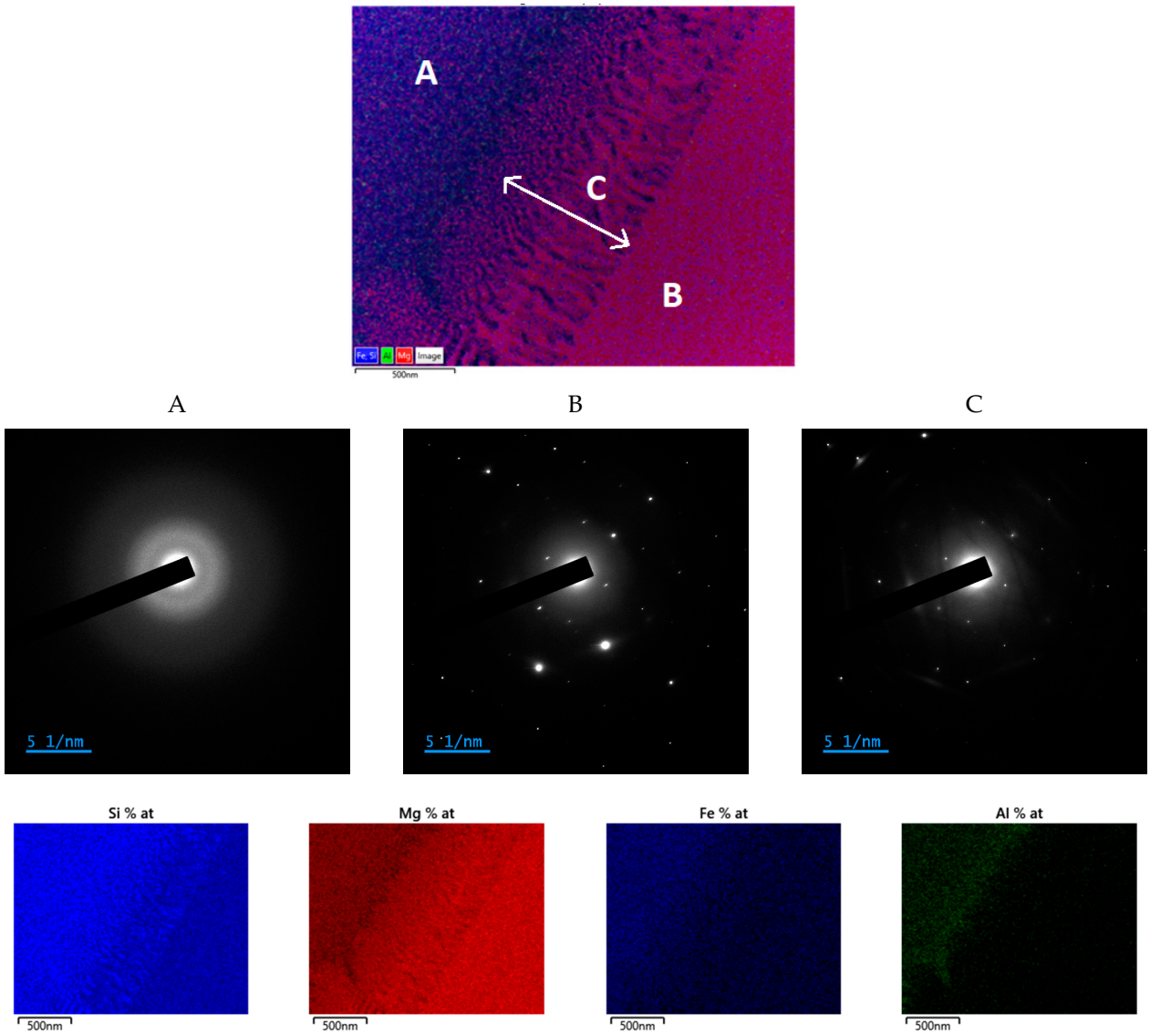

Figure 7. STEM-EDS image of the native slag, diffraction images of the different areas (A, B and C) of the sample and elemental mapping by element.

The elemental composition of each area was determined (using the average of 20 points for each area on two different TEM images):

- Area A, amorphous: Mg/Si = 0.41; Fe/Si = 0.21; Al/Si = 0.13. The Mg/Si ratio is very close to the one calculated with the mass balance (Section 3.2.2); the other two ratios are slightly higher with this technique. However, it confirms that aluminum is only detected in the amorphous phase.
- Area B, crystalline: Mg/Si = 1.8; Fe/Si = 0.2; (Mg + Fe)/Si = 2 and Mg/Fe = 10, which matches with the composition of forsterite determined by the Rietveld refinement: $Mg_{1.8}Fe_{0.2}SiO_4$ (Section 3.2.1).
- Area C, crystalline: Mg/Si = 1.3; Fe/Si = 0.1; (Mg + Fe)/Si = 1.4 and Mg/Fe = 10, which corresponds to no existing magnesium silicate and is probably a mixture of enstatite and forsterite.

Carbonated Slag

The TEM micrograph in Figure 8 shows that the carbonated slag is made up of very small particles that remain agglomerated after sonication. On the other hand, the fragility of the particles under the focused electron beam did not make it possible to reach higher magnification. Therefore, only STEM images and elemental mapping were performed on this sample. As seen in Figure 9, three different areas can also be observed, with different elemental compositions:

- Area A, crystalline, corresponds to carbonates and is mainly composed of magnesium, iron, carbon, and oxygen. As all EDS analyses revealed the presence of Mg and Fe in A, it was deduced that carbonates form a single mixed phase and do not separate magnesite from siderite. This is consistent with thermodynamic calculations, which indicate that the solid solution is the most stable [31]. However, the electron beam could not be correctly focused, and, therefore, EDS did not make it possible to verify the Mg/Fe ratio.
- Area B, crystalline, is mostly composed of magnesium, iron, and silica and, thus, probably corresponds to the residual forsterite.
- Area C, amorphous, is mainly composed of silica and alumina.

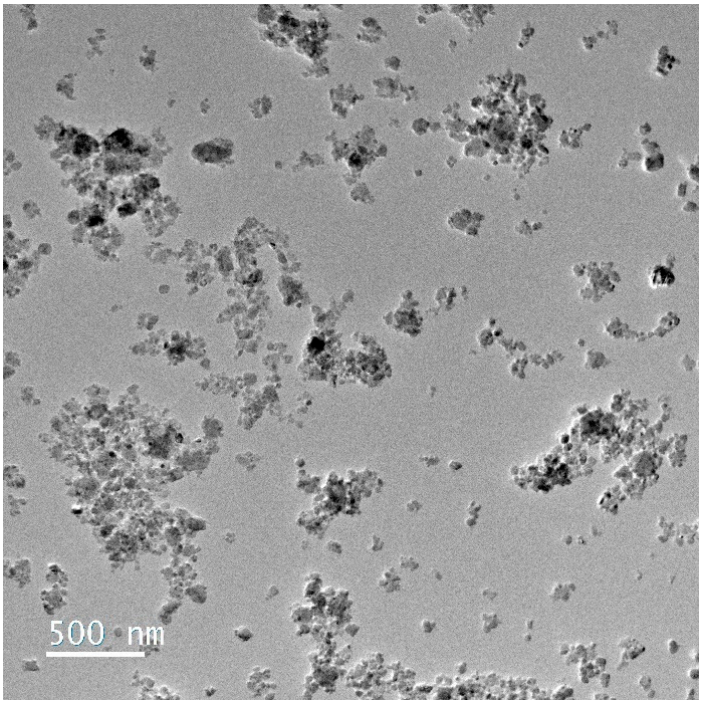

Figure 8. TEM images of carbonated slag.

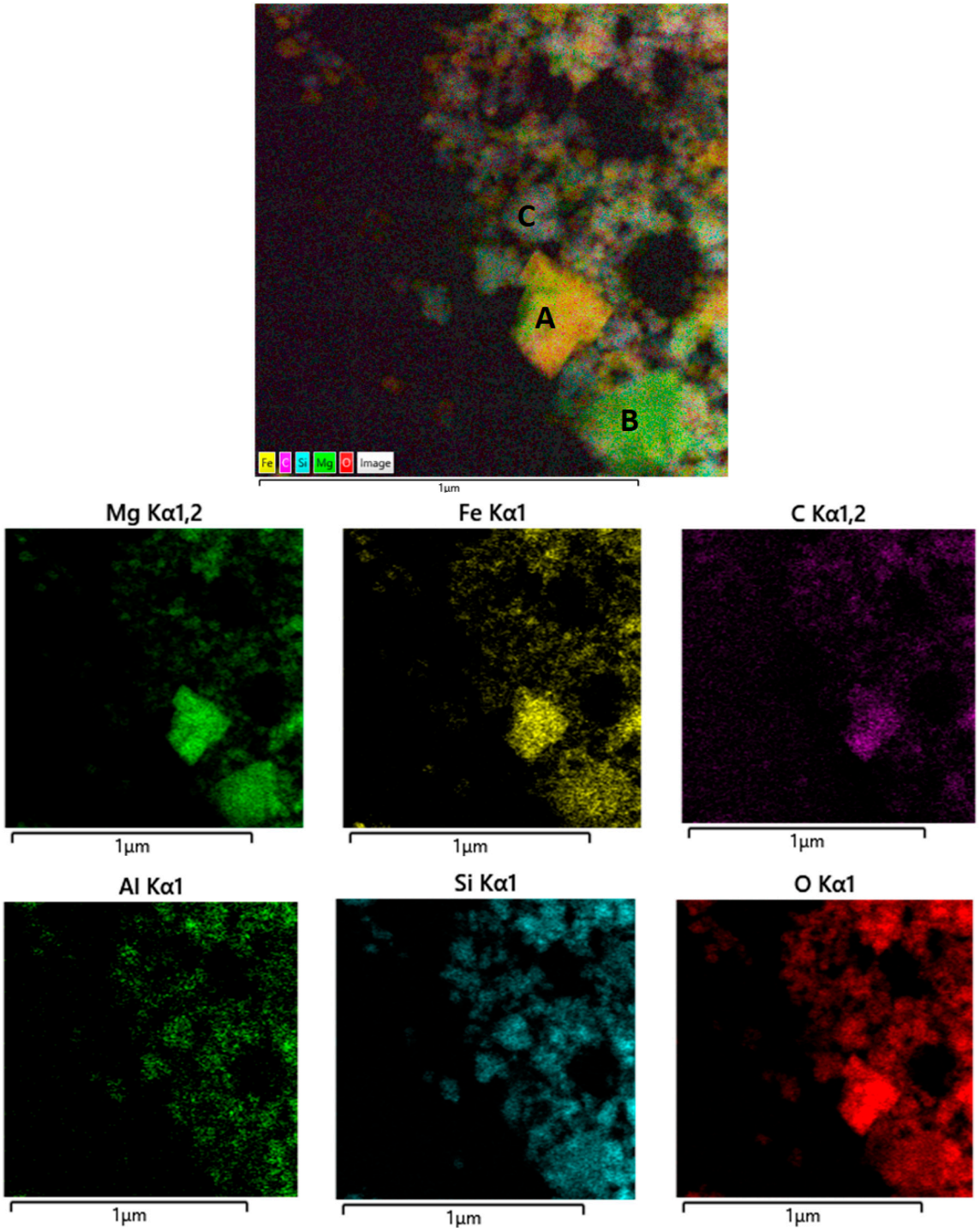

Figure 9. STEM-EDS image of the carbonated slag and elemental mapping by element.

3.3. Morphology

The native slag was granulated during the cooling step and had a size close to a grain of sand; therefore, this sample was crushed and sieved prior to the carbonation process. The carbonated slag was composed of very small particles (size around a few nm), which tended to agglomerate, as observed by TEM. Therefore, it was not possible to measure the size of the individual particles by using laser granulometry. Then, only the specific surface area was measured by using the BET method, which yielded 280 m^2/g, a very high value, in the order of magnitude of colloidal silica [32].

4. Discussion

4.1. Understanding the Carbonation Process

In this work, a panel of analytical techniques were used to characterize native and carbonated ferronickel slags. The characterization of both samples enabled a better understanding of the transformations during carbonation under attrition, in the following order: (a) to further improve the accelerated mineralization process, and (b) to consider the reuse of the carbonated products.

In this case study, the coupling of several conventional analytical techniques was very efficient to elucidate the composition of the complex multiphase materials. The two diagrams in Figure 10 represent the composition of the native and carbonated slags. The native slag is composed of three different phases: forsterite ferroan with a Mg/Fe ratio of 9 ($Mg_{1.8}Fe_{0.2}SiO_4$), an amorphous magnesium silicate also containing iron and aluminum with a Si/(Mg + Fe) ratio around 2, and a small amount of clinoenstatite ($MgSiO_3$), which is present at the interface between the forsterite and the amorphous phase. All phases are intimately mixed in the ferronickel slag. The presence of a high content of glassy phase in the native slag is explained by the phase diagram in Figure 11 [33]. The temperature in the electric arc furnace is between 1500 and 1700 °C during the manufacture of ferronickel. In this temperature range, the molten slag forms a mixture of forsterite and liquid. The material characterized in this study, which was obtained from the society Le Nickel, is quenched by sea water on its way out of the furnace. Therefore, the liquid transforms into a glassy phase. If the slag had been cooled down slowly, the product would have been crystalline and contained a mixture of enstatite and forsterite. The literature reports that the amorphous phase might be a magnesium silicate with the formula $(Mg,Fe)Si_2O_5$ [34]. This formula is in close agreement with the ratio of the element calculated in this study.

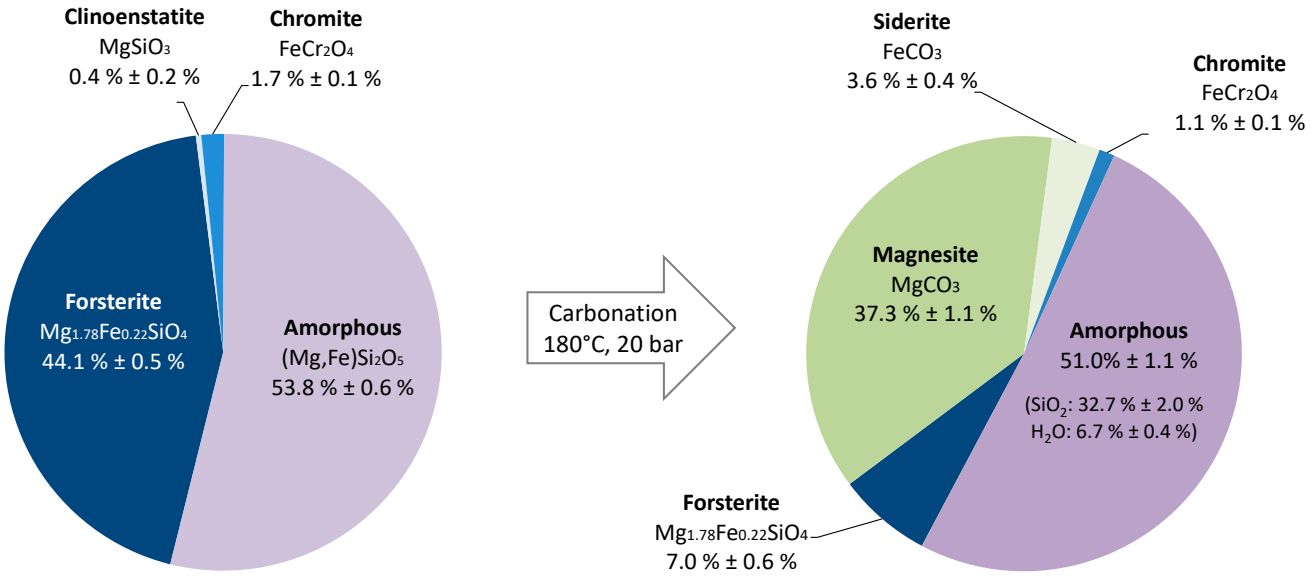

Figure 10. Quantitative mineralogical composition of the native and carbonated slags.

The carbonated product is composed of residual forsterite, a mixed magnesium and iron carbonate, and a hydrated amorphous silica containing a slight amount of aluminum. The amorphous silica contains 0.7 water per SiO_2 unit. The carbonation reactions of the slag components, thus, obeyed the following stoichiometric equations:

$$MgSi_2O_5 + CO_2 + 1.4\ H_2O \rightarrow MgCO_3 + 2\ SiO_2.0.7H_2O$$

$$Mg_{1.8}Fe_{0.2}SiO_4 + 2\ CO_2 + 0.7\ H_2O \rightarrow 1.8\ MgCO_3 + 0.2\ FeCO_3 + SiO_2.0.7H_2O$$

The characterization made on the samples showed that the initial amorphous magnesium silicate coming from the native slag had totally reacted during the carbonation process, whereas the crystalline forsterite was partially transformed, and, thus, a small amount of this forsterite was still present in the carbonated product. This means that this amorphous phase dissolved somewhat faster than forsterite.

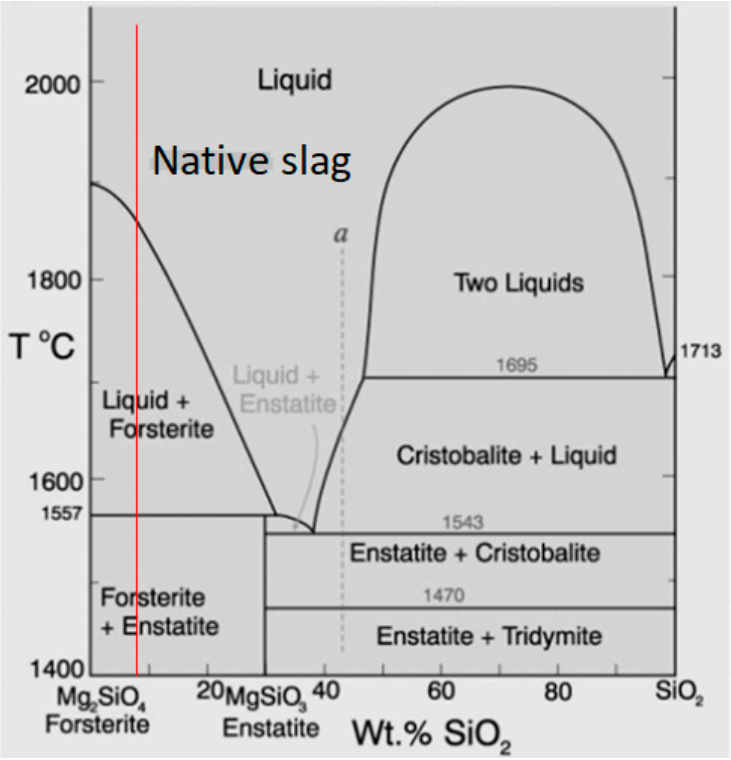

Figure 11. Phase diagram of forsterite and silica [33]. Vertical red line stands for the native slag.

In addition, the carbonated slag is composed of submicronic particles that tend to agglomerate, resulting in a very high specific surface (around 280 m^2/g). Dealing with this parameter is primordial for further reuse of the material in the construction sector and will be a real challenge.

4.2. The Reuse of Carbonated Slag

The characterization of the carbonated slag was a starting point to consider its reuse paths. In fact, this type of product could be interesting in the cement industry, considering its abundance and composition. The cement industry accounts for 8% of the global CO_2 emissions [35]. The stakeholders in this industry had already thought about solutions to reduce their environmental impact, such as switching to alternative fuels, using more efficient energy sources, etc. Other solutions that are proposed consist of using alternative binders or partially replacing the clinker in cement or in concrete manufacturing by materials with a lower environmental impact. Bourgeois et al. gave more details about the solutions that could be brought about by an integrated mineralization process [17]. Considering the composition of the carbonated products, their use as a material for the partial replacement of clinker or cement is relevant, as well as their use as a magnesium silicate binder.

4.3. Carbonated Slag as Pozzolanic Material

The carbonated product comprises amorphous silica, which is well known in the literature to be reactive in a cementitious environment [36] and is already used to partially replace the clinker. Amorphous silica is usually a fine powder coming from the ferro-silicate

industry and is referenced in the literature as silica fume. This material is also known to have a pozzolanic behavior in a cement medium, contributing to the long-term mechanical performance of the binder. Therefore, considering the composition of the carbonated product and the literature about silica additions in cement, this material should behave like a pozzolanic material in a cement environment. Trials were carried out by Bourgeois et al. [17]. The authors showed that it is possible to replace 20% of cement with the carbonated slag in a normalized mortar (with a superplasticizer) and to improve the mechanical strength of the material because of the pozzolanic reactivity of the carbonated product. Nonetheless, the fineness of the carbonated slag raises rheological issues. In addition, the characterization study was performed on only one product obtained after 24 h of carbonation, but products obtained at shorter reaction times and, thus, with lower carbonation yields—for instance, about 50% after 5 h at 150 °C and 10 bar of CO_2 [22]—should also be considered since they would allow one to reduce the process of energy penalty. A complete study on the replacement of Portland cement with different carbonated ferronickel slags will be carried out to determine the benefit of such an addition.

4.4. Carbonated Slag as Magnesium-Silicate Binder

The carbonated product contains amorphous silica but also magnesium carbonate, which could form magnesium oxide (periclase) after heating. Yet, magnesium silicate binders are prepared from a mixture of magnesium oxide and amorphous silica [37]. Therefore, the carbonated product could be a precursor of the synthesis of magnesium silicate binders. Preliminary experiments were carried out to determine whether it is possible to synthesize periclase (MgO) and within which temperature range. The decarbonation of magnesite starts from 500 °C (Figure 12); between 500 and 600 °C, magnesite is transformed in periclase, but at higher temperatures, only magnesioferrite ($MgFe_2O_4$) is formed. Then, to prepare a silico-magnesium binder, it is necessary to maintain the processing temperature between 500 and 600 °C.

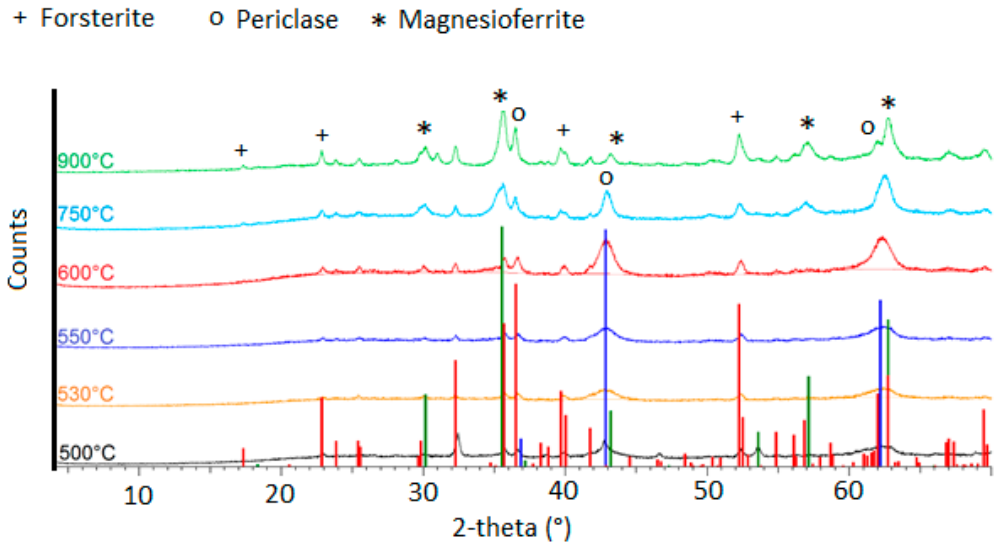

Figure 12. X-ray diffractograms of the carbonated slag heated at different temperatures. Vertical lines stand for forsterite (red lines), periclase (blue lines) and magnesioferrite (green lines).

Finally, a paste was prepared with a material prepared after treatment for 1 h at 600 °C, using a liquid-to-binder ratio of 1.2. After 7 days, the paste was characterized by XRD (Figure 13), and the presence of M-S-H was confirmed. These results are very promising, and a further study will be carried out.

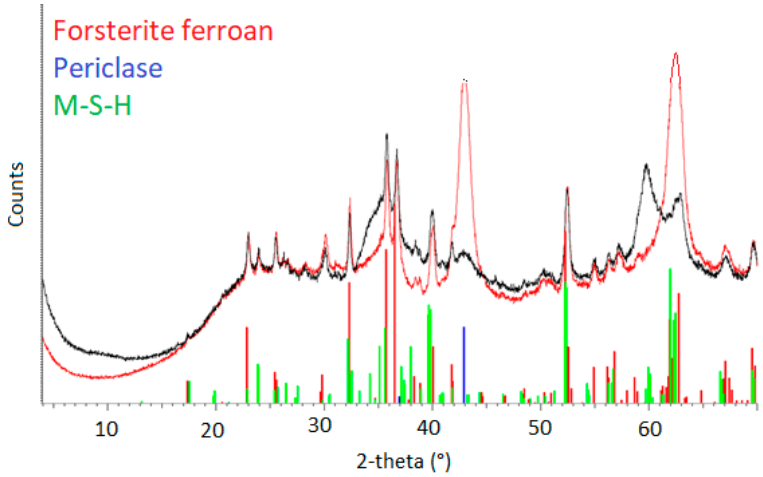

Figure 13. XRD diffractograms of the carbonation product treated at 600 °C before (red spectrum) and after 7 days of hydration (black spectrum).

5. Conclusions

This study aimed to fully characterize ferronickel slag from New Caledonia prior to and after a direct aqueous carbonation process. Several analytical techniques could identify crystalline and amorphous phases in both materials and quantify them. The methods used included chemical characterizations through ICP-AES and TGA-MS analyses, mineral characterizations provided by Q-XRD, FT-IR, and EDS coupled to electronic microscopy, and morphology characterizations using SEM and BET analysis.

These methods were successfully applied to identify and quantify the composition of a ferronickel slag from New Caledonia and its carbonated product. The native ferronickel slag is composed of 44 wt. % of forsterite iron, with a 1:4 Fe:Mg ratio and 54 wt. % of an amorphous phase with $(Mg,Fe)(Si,Al)_2O_5$ stoichiometry. The native slag also contains some traces of clinoenstatite and 1.7 wt. % of chromite. After 24 h of aqueous carbonation using an attrition-leaching process operated at 180 °C and 20 bar, the amorphous phase contained in the native slag totally reacted, whereas 7 wt. % forsterite iron remained in the carbonated material. The main reaction products are magnesite (37 wt. %) and siderite (3.6 wt. %) in the form of a solid solution and amorphous silica comprising some aluminum originating from the glassy phase in the slag (51 wt. %). Therefore, the full characterization of materials made it possible to understand the carbonation process. It was also used to define possible valorization paths for the products, as the carbonated product contains a high amount of amorphous silica, which makes it suitable for pozzolanic reactions in cementitious systems. On the other hand, this study shows that it is possible to synthesize a magnesium silicate binder after the decarbonation of magnesite at a very low temperature.

Author Contributions: Conceptualization, P.L., A.D., F.B., C.J. and M.C.; methodology, P.L., A.D., F.B., C.J. and M.C.; formal analysis, P.L. and M.C.; investigation, P.L. and A.D.; writing—original draft preparation, P.L.; writing—review and editing, F.B., C.J. and M.C.; visualization, P.L. and M.C.; supervision, F.B., C.J. and M.C.; project administration, F.B.; funding acquisition, F.B. All authors have read and agreed to the published version of the manuscript.

Funding: This work was part of a multi-disciplinary research effort co-funded by the New Caledonian Energy Agency ACE (grant #CS17-3160-00) and the French Environment and Energy Management Agency ADEME (grant #1894C0021).

Data Availability Statement: Data are available on request to the corresponding author.

Conflicts of Interest: The authors declare no conflict of interest.

References

1. IEA. *Technology Roadmap—Low-Carbon Transition in the Cement Industry*; IEA: Paris, France, 2018. Available online: https://www.iea.org/reports/technology-roadmap-low-carbon-transition-in-the-cement-industry (accessed on 3 May 2019).
2. Ben Haha, M.; Lothenbach, B.; Le Saout, G.; Winnefeld, F. Influence of slag chemistry on the hydration of alkali-activated blast-furnace slag—Part II: Effect of Al_2O_3. *Cem. Concr. Res.* **2012**, *42*, 74–83. [CrossRef]
3. Lavergne, F.; Belhadi, R.; Carriat, J.; Fraj, A.B. Effect of nano-silica particles on the hydration, the rheology and the strength development of a blended cement paste. *Cem. Concr. Compos.* **2019**, *95*, 42–55. [CrossRef]
4. Maragkos, I.; Giannopoulou, I.P.; Panias, D. Synthesis of ferronickel slag-based geopolymers. *Miner. Eng.* **2009**, *22*, 196–203. [CrossRef]
5. Bouasria, M.; Babouri, L.; Khadraoui, F.; Chateigner, D.; Gascoin, S.; Pralong, V.; Benzaama, M.H.; Orberger, B.; El Mendili, Y. Insights into the partial replacement of cement by ferronickel slags from New Caledonia. *Eur. J. Environ. Civ. Eng.* **2022**, *26*, 3662–3680. [CrossRef]
6. Yang, T.; Yao, X.; Zhang, Z. Geopolymer prepared with high-magnesium nickel slag: Characterization of properties and microstructure. *Constr. Build. Mater.* **2014**, *59*, 188–194. [CrossRef]
7. Balomenos, E.; Panias, D.; Mud, R. Iron recovery and production of high added value products from the metallurgical by-products of primary aluminum and ferro-nickel industries. In Proceedings of the 3rd International Slag Valorisation Symposium, Belgium, Leuven, 19–20 March 2013; pp. 161–172.
8. Komnitsas, K.; Zaharaki, D.; Perdikatsis, V. Effect of synthesis parameters on the compressive strength of low-calcium ferronickel slag inorganic polymers. *J. Hazard. Mater.* **2009**, *161*, 760–768. [CrossRef] [PubMed]
9. Le Nickel—SNL. FNS: A Promising Construction Material for the Pacific Region. 2017. Available online: http://sln.nc/sites/default/files/flippingbook/slnslg/fichiers/assets/common/downloads/publicati622on.pdf (accessed on 3 May 2019).
10. Yang, T.; Wu, Q.; Zhu, H.; Zhang, Z. Geopolymer with improved thermal stability by incorporating high-magnesium nickel slag. *Constr. Build. Mater.* **2017**, *155*, 475–484. [CrossRef]
11. Zhang, Z.; Zhu, Y.; Yang, T.; Li, L.; Zhu, H.; Wang, H. Conversion of local industrial wastes into greener cement through geopolymer technology: A case study of high-magnesium nickel slag. *J. Clean. Prod.* **2017**, *141*, 463–471. [CrossRef]
12. Wang, Q.; Yu, C.; Yang, J.; Chong, L.; Xu, X.; Wu, Q. Influence of nickel slag powders on properties of magnesium potassium phosphate cement paste. *Constr. Build. Mater.* **2019**, *205*, 668–678. [CrossRef]
13. Wu, Q.; Wu, Y.; Tong, W.; Ma, H. Utilization of nickel slag as raw material in the production of Portland cement for road construction. *Constr. Build. Mater.* **2018**, *193*, 426–434. [CrossRef]
14. Shoya, M.; Aba, M.; Tsukinaga, Y.; Tokuhashi, K. Frost resistance and air void system of self-compacting concrete incorporating slag as a fine aggregate. *ACI Spec. Publ.* **2003**, *212*, 1093–1108.
15. Sakoi, Y.; Aba, M.; Tsukinaga, Y.; Nagataki, S. Properties of concrete used in ferronickel slag aggregate. In Proceedings of the 3rd International Conference on Sustainable Construction Materials and Technologies, Japan, Tokyo, 18–21 August 2013; pp. 1–6.
16. Yang, T.; Zhang, Z.; Wang, Q.; Wu, Q. ASR potential of nickel slag fine aggregate in blast furnace slag-fly ash geopolymer and Portland cement mortars. *Constr. Build. Mater.* **2020**, *262*, 119990. [CrossRef]
17. Bourgeois, F.; Laniesse, P.; Cyr, M.; Julcour, C. Definition and exploration of the integrated CO_2 mineralization technological cycle. *Front. Energy Res.* **2020**, *8*, 113. [CrossRef]
18. Julcour-Lebigue, C.; Bourgeois, F.; Bonfils, B.; Benhamed, I.; Guyyot, F.; Bodénan, F.; Petito, C.; Gaucher, E.C. Development of an attrition leaching hybrid process for direct aqueous mineral carbonation. *Chem. Eng. J.* **2015**, *262*, 716–726. [CrossRef]
19. Seetharaman, S. (Ed.) *Treatise on Process Metallurgy, Vol. 3: Industrial Processes*; Elsevier: Amsterdam, The Netherlands, 2014. [CrossRef]
20. Huang, Y.; Wang, Q.; Shi, M. Characteristics and reactivity of ferronickel slag powder. *Constr. Build. Mater.* **2017**, *156*, 773–789. [CrossRef]
21. Julcour, C.; Cassayre, L.; Benhamed, I.; Diouani, J.; Bourgeois, F. Insights Into Nickel Slag Carbonation in a Stirred Bead Mill. *Front. Chem. Eng.* **2020**, *2*, 588579. [CrossRef]
22. Dufourny, A.; Julcour, C.; Esvan, J.; Cassayre, L.; Laniesse, P.; Bourgeois, F. Observation of the depassivation effect of attrition on magnesium silicates direct aqueous carbonation products, Sec. Negative Emission Technologies. *Front. Clim.* **2022**, *4*, 946735. [CrossRef]
23. National Institute of Standards and Technology. Physical Measure Laboratory, X-ray form Factor. Attenuation and Scattering Tables. Available online: https://physics.nist.gov/PhysRefData/FFast/html/form.html (accessed on 11 April 2022).
24. Toby, B.H. R factor in Rietveld analysis: How good is good enough? *Powder Diffr.* **2016**, *21*, 67–70. [CrossRef]
25. Choudhary, R.; Venkatraman, S.K.; Bulygina, I.; Chatterjee, A.; Abraham, J.; Senatov, F.; Kaloshkin, S.; Ilyasov, A.; Abakumov, M.; Knyazeva, M.; et al. Impact of forsterite addition on mechanical and biological properties of composites. *J. Asian Ceram. Soc.* **2020**, *8*, 1051–1065. [CrossRef]
26. Nojehdehi, A.M.; Moghaddam, F.; Hamedani, M.T. Mechanical properties of glass ionomer cement incorporating forsterite nanoparticles synthesized by the sol-gel method. *J. Sol-Gel Sci. Technol.* **2023**, *107*, 161–169. [CrossRef]
27. Oh, K.D.; Morikawa, H.; Iwai, S.; Aoki, H. The crystal structure of magnesite. *Am. Mineral.* **1973**, *58*, 1029–1033.
28. Dubrawski, J.V.; Channon, A.L.; Warne, S.S.J. Examination of the siderite-magnesite mineral series by Fourier transform infrared spectroscopy. *Am. Mineral.* **1989**, *74*, 187–190.

29. Santillán, J.; Catalli, K.; Williams, Q. An infrared study of carbon-oxygen bonding in magnesite to 60 GPa. *Am. Mineral.* **2005**, *90*, 1669–1673. [CrossRef]
30. Ellerbrock, R.; Stein, M.; Schaller, J. Comparing amorphous silica, short-range-ordered silicates and silicic acid species by FTIR. *Sci. Rep.* **2022**, *12*, 11708. [CrossRef] [PubMed]
31. Cassayre, L.; Bourgeois, F.; Julcour-Lebigue, C.; Benhamed, I.; Diouani, J.; Nahdi, K. Defining the operating conditions of the attrition-leaching process using thermodynamic process modelling. In Proceedings of the International Mineral Processing Congress IMPC 2016: XXVII, Québec, QC, Canada, 11–15 September 2016. Ref. GHGT14.
32. Gore, A.Y.; Banker, G.S. Surface chemistry of colloidal silica and possible application to stabilize aspirin in solid matrixes. *J. Pharm. Sci.* **1979**, *62*, 197–202. [CrossRef] [PubMed]
33. Bowen, N.L.; Anderson, O. The binary system: MgO-SiO_2. *Am. J. Sci.* **1914**, *37*, 487–500. [CrossRef]
34. Umemoto, K. Phase transitions in $MgSiO_3$ post-perovskite in super-Earth mantles. *Earth Planet. Sci. Lett.* **2017**, *478*, 40–45. [CrossRef]
35. Schneider, M.; Romer, M.; Tschudin, M.; Bolio, H. Sustainable cement production—Present and future. *Cem. Concr. Res.* **2011**, *41*, 642–650. [CrossRef]
36. Fidjestøl, P.; Lewis, R. *Microsilica as an Addition, Lea's Chemistry of Cement and Concrete*, 4th ed.; Elsevier: Amsterdam, The Netherlands, 1998; pp. 679–712. [CrossRef]
37. Walling, S.A.; Provis, J.L. Magnesia-Based Cements: A Journey of 150 Years, and Cements for the Future? *Chem. Rev.* **2016**, *116*, 4170–4204. [CrossRef]